



Journal
of

Contaminant Hydrology

Editors

E.O. Frind, Waterloo (Canada)

P.L. Bjerg, Lyngby (Denmark)

S.B. Haderlein, Tübingen (Germany)

A.J. Valocchi, Urbana, IL (U.S.A.)

This article was originally published in a journal published by Elsevier, and the attached copy is provided by Elsevier for the author's benefit and for the benefit of the author's institution, for non-commercial research and educational use including without limitation use in instruction at your institution, sending it to specific colleagues that you know, and providing a copy to your institution's administrator.

All other uses, reproduction and distribution, including without limitation commercial reprints, selling or licensing copies or access, or posting on open internet sites, your personal or institution's website or repository, are prohibited. For exceptions, permission may be sought for such use through Elsevier's permissions site at:

<http://www.elsevier.com/locate/permissionusematerial>

Modeling in-situ uranium(VI) bioreduction by sulfate-reducing bacteria

Jian Luo^{a,*}, Frank-Andreas Weber^b, Olaf A. Cirpka^c, Wei-Min Wu^a,
Jennifer L. Nyman^a, Jack Carley^d, Philip M. Jardine^d,
Craig S. Criddle^a, Peter K. Kitanidis^a

^a *Stanford University, Department of Civil and Environmental Engineering, Stanford, CA 94305-4020, USA*

^b *Swiss Federal Institute of Technology (ETH) Zürich, Institute of Terrestrial Ecology, ETH Zentrum CHN, CH-8092 Zürich, Switzerland*

^c *Swiss Federal Institute for Aquatic Science and Technology (EAWAG), Department of Water Resources and Drinking Water, Überlandstrasse 133, CH-8600 Dübendorf, Switzerland*

^d *Oak Ridge National Laboratory, Environmental Science Division, Oak Ridge, TN 37831-6038, USA*

Received 27 July 2005; received in revised form 28 September 2006; accepted 3 January 2007

Available online 12 January 2007

Abstract

We present a travel-time based reactive transport model to simulate an in-situ bioremediation experiment for demonstrating enhanced bioreduction of uranium(VI). The model considers aquatic equilibrium chemistry of uranium and other groundwater constituents, uranium sorption and precipitation, and the microbial reduction of nitrate, sulfate and U(VI). Kinetic sorption/desorption of U(VI) is characterized by mass transfer between stagnant micro-pores and mobile flow zones. The model describes the succession of terminal electron accepting processes and the growth and decay of sulfate-reducing bacteria, concurrent with the enzymatic reduction of aqueous U(VI) species. The effective U(VI) reduction rate and sorption site distributions are determined by fitting the model simulation to an in-situ experiment at Oak Ridge, TN. Results show that (1) the presence of nitrate inhibits U(VI) reduction at the site; (2) the fitted effective rate of in-situ U(VI) reduction is much smaller than the values reported for laboratory experiments; (3) U(VI) sorption/desorption, which affects U(VI) bioavailability at the site, is strongly controlled by kinetics; (4) both pH and bicarbonate concentration significantly influence the sorption/desorption of U(VI), which therefore cannot be characterized by empirical isotherms; and (5) calcium–uranyl–carbonate complexes significantly influence the model performance of U(VI) reduction.

© 2007 Elsevier B.V. All rights reserved.

Keywords: Uranium reduction; Sulfate reduction; Surface complexation model; Reactive transport; Inhibition

* Corresponding author. Present address: School of Civil and Environmental Engineering, Georgia Institute of Technology, Atlanta, GA 30332-0355, USA.

E-mail address: jianluo@ce.gatech.edu (J. Luo).

1. Introduction

In the past decade, uranium contamination of groundwater and its remediation have received increased attention. The oxidation state of uranium strongly influences its solubility and mobility, i.e., U(VI) complexes are much more soluble and mobile than U(IV) complexes. Under aerobic conditions in natural waters, U(VI) exists predominantly as the uranyl ion, UO_2^{2+} at $\text{pH} < 5.0$ and forms various uranyl–carbonate species at $\text{pH} > 5$ (Grenthe et al., 1992). In contrast, tetravalent uranium, U(IV), precipitates as highly insoluble uraninite, UO_2 , in aquifers (Parks and Pohl, 1988). Thus, microbial reduction of U(VI) under anaerobic conditions provides a promising bioremediation approach to immobilize uranium within contaminated aquifers (Lovley et al., 1991). Laboratory experiments and field investigations have shown that Fe(III)-reducing bacteria (FeRB) and some sulfate-reducing bacteria (SRB), among others, are capable of reducing soluble U(VI) to insoluble U(IV), therefore immobilizing dissolved uranium in aquifers (e.g., Lovley et al., 1991; Lovley and Phillips, 1992a,b).

Most published research reports have been focused on bioreduction of U(VI) by various microbial cultures at laboratory scale (e.g., Lovley et al., 1991; Lovley and Phillips, 1992a,b; Gorby and Lovley, 1992; Ganesh et al., 1997; Truex et al., 1997; Abdelouas et al., 1998; Fredrickson et al., 2000; Fredrickson et al., 2002; Holmes et al., 2002). Kinetics have been analyzed for defined or mixed cultures in laboratory (e.g., Liger et al., 1999; Spear et al., 1999, 2000). Under field conditions, U(VI) undergoes hydrological, geochemical, and biological processes in complex interaction, such as sorption/desorption, advective-dispersive transport, and microbial transformations. Uranium sorption/desorption is significantly influenced by bicarbonate concentrations and pH (Waite et al., 1994; Wazne et al., 2003). At the sorption sites, uranium competes with other ions. Since the geochemical environment may vary over the course of the experiment, simplified approaches to model U(VI) sorption, such as the assumption of a linear retardation factor, appear insufficient (Bain et al., 2001). For bioreduction of U(VI), nitrate, Fe (III) and sulfate serve as competing electron acceptors which should be considered in the simulations (e.g., Wielinga et al., 2000; North et al., 2004; Wu et al., 2005). In the presence of significant calcium concentrations, the highly stable but poorly biodegradable calcium–uranyl–carbonate complexes should also be included in the simulation (Bernhard et al., 1996; Kalmykov and Choppin, 2000; Bernhard et al., 2001; Brooks et al., 2003).

Kinetics of microbial U(VI) reduction have been described by several investigators for defined and mixed cultures. Liger et al. (1999) formulated the kinetics of surface-catalyzed U(VI) reduction by Fe(II) on hematite. Assuming U(VI) as the sole electron acceptor, Spear et al. (1999) proposed Michaelis–Menten kinetics to model U(VI) reduction by SRB. When considering both U(VI) and sulfate as electron acceptors, Spear et al. (2000) described U(VI) and sulfate reduction by first-order and zeroth-order kinetics, respectively. Liu et al. (2001) proposed reaction kinetics for Fe(III) reduction, which is of first order with respect to the available surface site concentration of Fe(III). Weber (2002) extended the model of Liu et al. (2001) to growth conditions and applied it to U(VI) reduction simulations. Wu et al. (2005) indicated that the U(VI) reduction can be well simplified as a first-order reaction at U(VI) below 50 mg/l by a denitrifying biomass. Nagpal et al. (2000) studied the kinetics of ethanol utilization by SRB.

To describe U(VI) sorption/desorption, surface complexation models (SCMs), which assume local equilibrium, have been developed mainly for relatively well-defined pure material phases, e.g., Fe(III) oxides and hydroxides (Tripathi, 1984; Hsi and Langmuir, 1985; Waite et al., 1994; Morrison et al., 1995), silicates (Kohler et al., 1996; Prikryl et al., 2001), aluminum oxides (Prikryl et al., 1994; McKinley et al., 1995), pyrite (Wersin et al., 1994) and reference clay

minerals (McKinley et al., 1995; Turner et al., 1996). Modelers have attempted to adapt such surface complexation models to describe sorption to heterogeneous subsurface material either following a principle component or component additivity approach (e.g., Barnett et al., 2002), or preferring a semi-empirical general composite approach (Davis et al., 1998, 2004). Giammar and Hering (2001) and Qafoku et al. (2005) investigated uranium sorption/desorption kinetics using column studies and observed strong kinetic effects, which they expressed in terms of half-lives of sorption/desorption ranging from hours to a week. Wang et al. (2003) studied the uncertainty of model parameters for uranium bioremediation considering kinetics of precipitation/dissolution described by a linear isotherm. So far, no appropriate model combining aquatic equilibrium chemistry of uranium, bioreduction kinetics, kinetic uranium sorption/desorption using surface complexation models and transport has yet been developed to simulate in-situ U(VI) bioreduction. Wang and Papenguth (2001) have derived a framework that couples microbial metabolism with redox chemistry of radionuclides. Roden and Scheibe (2005) present a conceptual and numerical model to describe U(VI) reduction by metal reducing bacteria in fractured subsurface sediments. Their simulations lack the test of experimental data.

In this study, we develop a reactive transport model to simulate an in-situ bioreduction experiment of U(VI) in an aquifer in Oak Ridge, TN, which is contaminated by high concentrations of uranium and nitric acid. The model considers aquatic equilibrium chemistry of uranium and other groundwater constituents, competitive uranium sorption and precipitation, and kinetic microbial reduction of nitrate, sulfate and U(VI). Kinetic sorption/desorption of U(VI) is characterized by mass transfer between stagnant micro-pores and mobile flow zones. For transport calculation, a travel-time based approach is applied to model advective-reactive transport. The model is implemented in the computer code PHREEQC (Parkhurst and Appelo, 1995), distributed by the U.S. Geological Survey.

2. Bioremediation experiment

The bioremediation of uranium contaminated subsurface has been tested in Area 3 of the Field Research Center (FRC) of the Natural and Accelerated Bioremediation (NABIR) program of the U.S. Department of Energy (DOE) at the Y-12 National Security Complex at Oak Ridge, TN, as described elsewhere (Wu et al., 2006a,b). This site is adjacent to the former S-3 disposal ponds and has been characterized for its geochemistry, stratigraphy and hydrogeology (Fiene et al., 2004; Phillips et al., 2006). Groundwater at the site generally migrates in the unconsolidated intact saprolite, which is the main pathway of the contaminant plume and target of the biostimulation experiment. The groundwater is acidic (pH 3.4–3.9) and contains high levels of nitrate (10 g/l) and high concentrations of a wide range of metals, including Al, Ca, Mg, Na, and Ni. Soluble uranium is present at highly toxic levels of 20–50 mg/l. Uranium content in sediments is up to 700 mg/kg.

Fig. 1 shows a plan view of the multiple-well system installed at the site. A four-well system, including two injection wells: FW024 and FW104, and two extraction wells: FW026 and FW103, was installed to create a nested inner cell, functioning as an in-situ reactor for the U(VI) bioreduction experiment (Luo et al., 2006b; Wu et al., 2006a). Well screens are located at depth 11–14 m, the fast flow zone with high hydraulic conductivities identified by flowmeter tests (Fiene et al., 2004). Multilevel sampling wells (MLS) were installed in the middle of the well system.

We established a three-phase strategy to stimulate and maintain favorable anaerobic conditions (Wu et al., 2006a). In phase I (day 9–136), the bulk nitrate and Ca were washed out by an acidic, aluminum-free solution, because these water constituents inhibit uranium bioreduction (Abdelouas

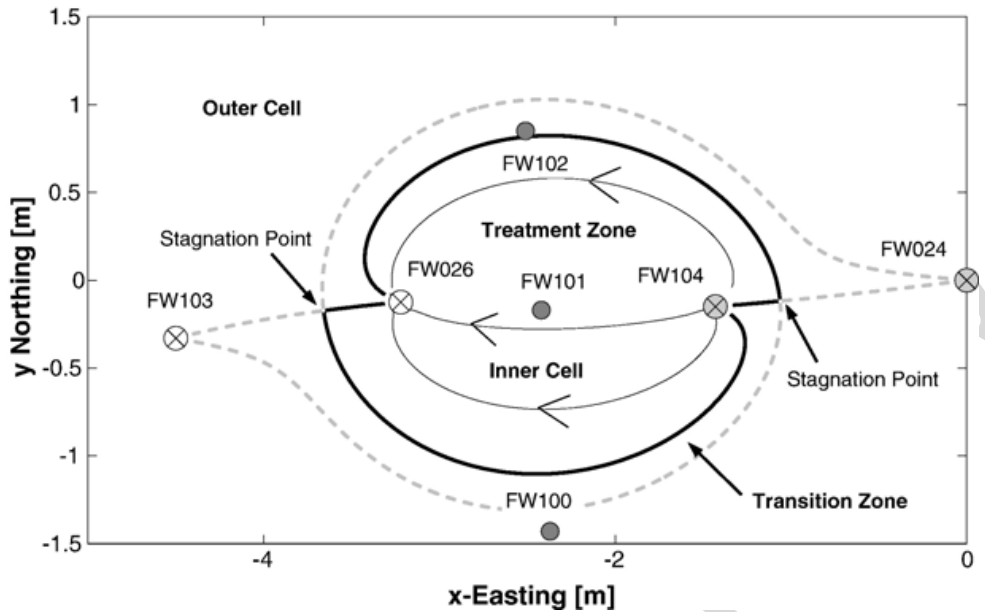


Fig. 1. Plan view of the treatment zone created by the installed multiple-well system. The black thick lines, passing through stagnation points, delineate a nested inner cell functioning as the treatment zone, where the lines with arrows indicate flow directions, and the grey dashed lines are the separation streamlines delineating the outer zones. FW024 and FW104 are the injection wells, and FW026 and FW103 are extraction wells. FW100, FW101, and FW102 are MLS wells.

et al., 1998; Senko et al., 2002; Finneran et al., 2002; Brooks et al., 2003), then pH was raised to near-neutral conditions, which are favorable for U(VI)-reducing bacteria. In phase II (days 136–184), ethanol was introduced into the subsurface for denitrification of the remaining nitrate and for the stimulation of microbial activity. In phase III (days 185–480 and afterwards), ethanol was introduced intermittently for U(VI) reduction. Active microbial populations for denitrification, Fe(III) reduction and sulfate reduction were stimulated in the treatment area. Removal of nitrate and reduction of U(VI) was achieved (Wu et al., 2006a).

In this study, we focused on the MLS well and depth with the strongest response (FW101–2 in the fast flow zone) over the time course of one remediation experiment (i.e., one period of ethanol addition) to characterize the remediation process. More experimental results have been published elsewhere (Wu et al., 2006b), which show similar characteristics for each ethanol injection period. The test was performed during days 400–410. According to bacteria counts (most-probable-number enumeration) before and after the test (days 354 and 453), the microbial populations in FW101–2 were: 10^3 – 10^6 cells/ml denitrifiers, 10^4 – 10^5 cells/ml SRB, and 10^2 – 10^3 cells/ml FeRB (Wu et al., 2006b). This indicated that, around the sampled well, sulfate reducers were much more abundant than Fe reducers during the test period. Microbial community analysis indicated that *Desulfovibrio* spp. and *Geobacter* spp. were predominant SRB and FeRB in both sediment and groundwater samples. Thus, based on these evidence and indications, SRB are considered as the primarily responsible for U(VI) reduction (Wu et al., 2006b). A K_2CO_3 solution was injected to the recirculation line for 2 days prior ethanol injection in order to raise pH and enhance bioavailability of U(VI). Subsequently, ethanol was injected at a concentration of 1.3 mM into FW104 for 48 h. After the ethanol injection stopped, the injection of K_2CO_3 was maintained for 36 h. Samples were withdrawn from the injection well FW104 and the MLS well FW101–2 to monitor pH, alkalinity, nitrate, U(VI), sulfate and COD. During the test period, the temperature in the subsurface was 17–18 °C.

3. Model development

3.1. Reactive transport equations

In our simulations, local dispersion is neglected because practically all mixing takes place within the wells (Wu et al., 2006b). Some mixing is accounted for through the kinetics of the two-region model. For steady-state flow fields, the advective-reactive equations for the two-region model with equilibrium sorption are:

$$\frac{\partial c_m^i(t, \mathbf{x})}{\partial t} + \frac{\partial \overline{c_m^i}(t, \mathbf{x})}{\partial t} + \mathbf{v} \cdot \nabla c_m^i(t, \mathbf{x}) = r_m^i(t, \mathbf{x}) + \lambda_m [c_m^i(t, \mathbf{x}) - \overline{c_m^i}(t, \mathbf{x})] \quad (1)$$

$$\frac{\partial c_{im}^i(t, \mathbf{x})}{\partial t} + \frac{\partial \overline{c_{im}^i}(t, \mathbf{x})}{\partial t} = r_{im}^i(t, \mathbf{x}) + \lambda_{im} [c_m^i(t, \mathbf{x}) - c_{im}^i(t, \mathbf{x})] \quad (2)$$

where c_m^i and c_{im}^i are the dissolved concentrations in the mobile and immobile domains of species i , respectively; $\overline{c_m^i}$ and $\overline{c_{im}^i}$ are the sorbed concentrations in the mobile and immobile domains, expressed as mass of sorbed compound per volume of water; λ_m and λ_{im} are the first-order rate coefficients for mass transfer between the mobile and immobile domains; t is time; \mathbf{v} is the seepage velocity vector; \mathbf{x} is the vector of spatial coordinates; $r_m^i(t, \mathbf{x})$ and $r_{im}^i(t, \mathbf{x})$ are the reaction rates for i in the mobile and immobile domains, respectively.

Because the flow field created by the multiple-well system is nonuniform, \mathbf{v} varies in space. One can transform the multi-dimensional advection-reaction equation to a one-dimensional equation by solving transport along a streamline in travel-time coordinates $\tau(\mathbf{x})$:

$$\tau(\mathbf{x}) = \int_{x_{in}}^x \frac{d\xi}{\|\mathbf{v}_\xi\|} \quad (3)$$

in which ξ is the spatial coordinate along the velocity trajectory. Location \mathbf{x} and its corresponding travel time are related to the inflow boundary. At the injection point, \mathbf{x}_{in} , the travel time is zero. Substituting Eq. (3) into Eqs. (1) and (2) yields the travel-time based advection-reaction equation for the mobile domain (e.g., Simmons et al., 1995; Crane and Blunt, 1999; Cirpka and Kitanidis, 2000):

$$\frac{\partial c_m^i(t, \tau)}{\partial t} + \frac{\partial c_m^i(t, \tau)}{\partial \tau} + \frac{\partial \overline{c_m^i}(t, \tau)}{\partial t} = r_m^i(t, \tau) + \lambda_m [c_m^i(t, \tau) - \overline{c_m^i}(t, \tau)] \quad (4)$$

$$\frac{\partial c_{im}^i(t, \tau)}{\partial t} + \frac{\partial \overline{c_{im}^i}(t, \tau)}{\partial t} = r_{im}^i(t, \tau) + \lambda_{im} [c_m^i(t, \tau) - c_{im}^i(t, \tau)] \quad (5)$$

where each concentration is a function of time and, instead of location, travel time from the injection boundary. The boundary condition is $c_m^i(t, \tau=0) = c_m^i(t, \mathbf{x}_{in})$ and $c_{im}^i(t, \tau=0) = c_{im}^i(t, \mathbf{x}_{in})$, the concentrations at the injection point, which in our case are the measurements at the injection well FW104.

Biomass is assumed to be active only in the mobile domain, respiring only dissolved U(VI), sulfate, and nitrate. Thus, r_m^i includes aqueous speciation calculations, U(VI) sorption/desorption and bioreduction, and r_{im}^i includes the aqueous speciation calculations and the interaction with sorption sites. Sorption is described by a principal component SCM for competitive sorption onto ferrihydrite-like surfaces. Fractions, f_m and $f_{im} = 1 - f_m$, are used to describe the sorption site distribution in the mobile and immobile zones.

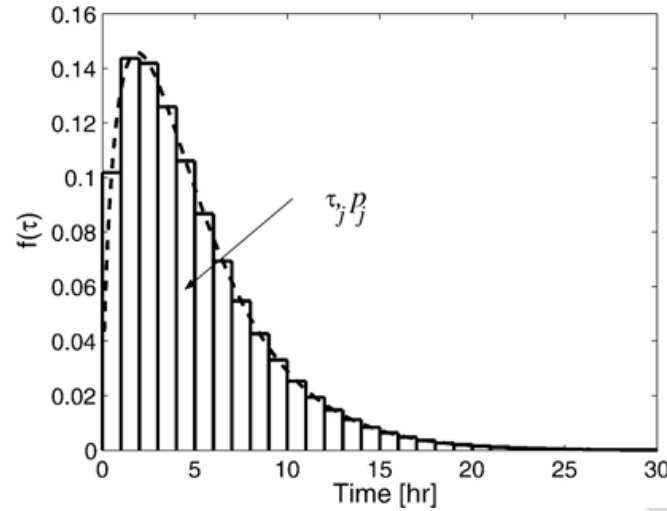


Fig. 2. Streamtube discretization based on travel-time *pdf*. Each streamtube is assigned with a mean travel time τ_j , and a flow probability p_j .

The methodology for solving the transport problem follows the methods presented by Cirpka and Kitanidis (2000). Fig. 2 illustrates the approach. A tracer test was implemented and used to generate the travel-time distributions from FW104 to FW101–2 by using a parametric approach (Luo et al., 2006a). Then, advective streamtubes with residence times τ_j and flow fraction p_j are introduced following the travel-time probability density function, f . Summation of the concentration of all the streamtubes gives the flux-averaged concentration at the observation point:

$$c_m^i(t) = \sum_j p_j(\tau_j) c_m^i(t|\tau_j) \quad (6)$$

where

$$p_j(\tau_j) = \frac{f_j \Delta \tau}{\sum f_j \Delta \tau} \quad (7)$$

3.2. Reaction kinetics

In the field experiment, SRB and FeRB are considered primarily responsible for U(VI) reduction. Anaerobic metabolism in aquifers exploits a succession of terminal electron accepting processes based on the redox potential of the electron acceptor, and generally a single terminal electron accepting process dominates (Froelich et al., 1979; Reeburgh, 1983). In the presence of nitrate, denitrification is dominant. When nitrate is depleted, microbial processes shift to Fe(III) reduction and then sulfate reduction, and during both periods U(VI) is reduced to U(IV) (Anderson and Lovley, 2002; Nyman et al., 2005). Ethanol was injected into the subsurface in this field experiment to stimulate microbial growth and subsequent U(VI) reduction. To simplify the model, the following assumptions are made:

- (1) U(VI) reduction during the test period (days 400–410) is solely attributed to SRB because the most probable numbers of these bacteria were by almost an order of magnitude larger than those of FeRB (Wu et al., 2006b) and because U(VI) reduction proceeded concurrently

Table 1
Kinetic parameters for bioreactions

Parameter	Value	References
Y_{NO_3}	0.2143 mol _{VSS} /mol _{EtOH} =0.53 mg _{VSS} /mg _{EtOH}	
Y_{SO_4}	0.06 mol _{VSS} /mol _{EtOH} =0.15 mg _{VSS} /mg _{EtOH}	
$F_{NO_3,EtOH}$	1.4143 mol _{Nitrate} /mol _{EtOH} =1.91 mg _{Nitrate} /mg _{EtOH}	
$F_{SO_4,EtOH}$	1.35 mol _{Sulfate} /mol _{EtOH} =2.82 mg _{Sulfate} /mg _{EtOH}	
$F_{U(VI),EtOH}$	6 mol _{U(VI)} /mol _{EtOH} =31 mg _{U(VI)} /mg _{EtOH}	
d_{NO_3}	4 mol _{Nitrate} /mol _{VSS} =2.20 mg _{Nitrate} /mg _{VSS}	
d_{SO_4}	2.5 mol _{Sulfate} /mol _{VSS} =2.13 mg _{Sulfate} /mg _{VSS}	
$d_{U(VI)}$	10 mol _{U(VI)} /mol _{VSS} =21 mg _{U(VI)} /mg _{VSS}	
f_d	0.8	(3)
q_{max,NO_3}	0.004 mg _{EtOH} /mg _{VSS} min	(5)
q_{max,SO_4}	0.0028 mg _{EtOH} /mg _{VSS} min	(4)
K_{NO_3}	0.2 mg _{Nitrate} /l	(1, 2)
K_{SO_4}	0.96 mg _{Sulfate} /l	(7)
$K_{U(VI)}$	119 mg _{U(VI)} /l	(6)
K_{EtOH,NO_3}	0.48 mg _{EtOH} /l	(5)
K_{EtOH,SO_4}	0.2 mg _{EtOH} /l	(4)
$K_{EtOH,U(VI)}$	0.04 mg _{EtOH} /l	(6)
b_N	0.05/day	(5)
b_S	0.05/day	(5)
b_U	0.05/day	

(1) Almeida et al. (1997); (2) Betlach and Tiedje (1981); (3) McCarty (1975); (4) Nyman (2006); (5) Rittmann and McCarty (2001); (6) Spear et al. (1999); (7) Wang et al. (2003).

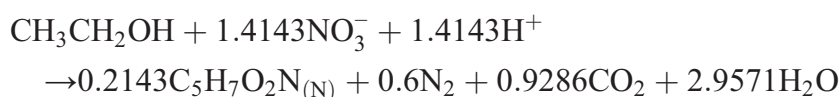
with sulfate reduction in microcosms with sediment from the site (Nyman et al., 2006; Nyman, 2006);

- (2) Reduction of nitrate is assumed to be controlled by dissimilative denitrification to N₂, catalyzed by denitrifying bacteria;
- (3) The energy produced from U(VI) reduction is not considered to support microbial growth because of comparably low levels of U(VI) in groundwater (<0.8 mg/l); and
- (4) The subsurface was maintained under anaerobic or anoxic conditions during the tests period and reoxidation of U(IV) by dissolved oxygen or other oxidants is ignored.

Therefore, the proposed model includes reactions of denitrification, sulfate reduction and U(VI) reduction as described in the following. Associated parameters are summarized in Table 1.

3.3. Denitrification

For the growth of denitrifying bacteria, we assume that 50% of the electron equivalents in ethanol is used for biosynthesis, $f_s=0.5$, while the other 50% is used for energy, $f_e=0.5$ (Rittmann and McCarty, 2001). Then, the overall reaction for denitrification due to ethanol consumption is:

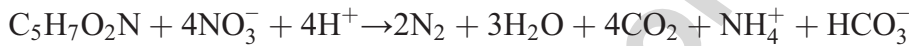


in which $C_5H_7O_2N$ is a virtual “molecule” of biomass, and the subscript (N) indicates nitrate reducers. The net growth rate of denitrifying biomass is related to the rate of nitrate reduction via the yield coefficient Y_{NO_3} [$M_x M_s^{-1}$]:

$$\begin{aligned} \frac{dX_N}{dt} = & Y_{NO_3} \frac{q_{\max,NO_3} c_{EtOH}}{K_{EtOH,NO_3} + c_{EtOH}} \frac{c_{NO_3}}{K_{NO_3} + c_{NO_3}} X_N - b_N X_N \frac{c_{NO_3}}{K_{NO_3} + c_{NO_3}} \\ & - b_S X_N \frac{c_{SO_4}}{K_{SO_4} + c_{SO_4}} \frac{K_{NO_3}}{K_{NO_3} + c_{NO_3}} - b_U X_N \frac{c_{U(VI)}^*}{K_{U(VI)} + c_{U(VI)}^*} \frac{K_{NO_3}}{K_{NO_3} + c_{NO_3}} \end{aligned} \quad (8)$$

where c_{EtOH} , c_{NO_3} , c_{SO_4} , $c_{U(VI)}^*$ are the concentrations of ethanol, nitrate, sulfate and bioavailable uranium(VI) [ML^{-3}]; q_{\max,NO_3} is the maximum specific rate of substrate utilization for nitrate [$M_s M_x^{-1} T^{-1}$]; K_{EtOH,NO_3} , K_{NO_3} , K_{SO_4} and $K_{U(VI)}$ are half saturation coefficients for ethanol, nitrate, sulfate and uranium(VI) [ML^{-3}]; X_N is the concentrations of active denitrifying bacteria [$M_x L^{-3}$]; and b_N , b_S , b_U are the cell decay rates with the electron acceptors nitrate, sulfate and uranium. The inhibition term $K_{NO_3}/(K_{NO_3} + c_{NO_3})$ is used to model the transition between the successive electron accepting processes, i.e., when nitrate concentrations drop to the value comparable to K_{NO_3} , sulfate and uranium(VI) become the prevailing electron acceptors for biomass decay.

Nitrate is consumed in the growth of the denitrifiers and in the decay of both denitrifiers and SRB. The reaction for biomass decay with nitrate as an electron acceptor is:



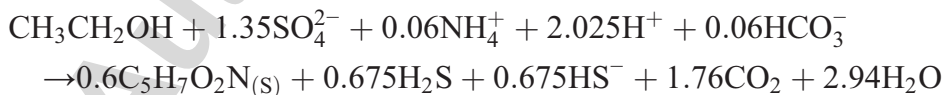
where $C_5H_7O_2N$ includes both denitrifying and SRB. The related rate of nitrate reduction is given by:

$$\begin{aligned} \frac{dc_{NO_3}}{dt} = & -q_{\max,NO_3} F_{NO_3,EtOH} \frac{c_{EtOH}}{K_{EtOH,NO_3} + c_{EtOH}} \frac{c_{NO_3}}{K_{NO_3} + c_{NO_3}} X_N \\ & - d_{NO_3} f_d (b_N X_N + b_S X_S) \frac{c_{NO_3}}{K_{NO_3} + c_{NO_3}} \end{aligned} \quad (9)$$

where X_S is the concentration of active SRB [$M_x L^{-3}$], d_{NO_3} is the nitrate demand for the cell decay [MM_x^{-1}], f_d is the fraction of cells that is biodegradable, and $F_{NO_3,EtOH}$ is the stoichiometric ratio of nitrate to ethanol utilization for biomass synthesis [MM_s^{-1}].

3.4. Sulfate reduction

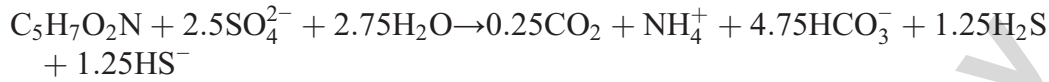
For SRB, we assume that 10% of the electron equivalents in ethanol is used for synthesis, $f_s=0.1$, while the other 90% is used for energy, $f_e=0.9$ (Rittmann and McCarty, 2001). Assuming that ethanol is completely degraded to CO_2 by sulfate reducers, the overall reaction for sulfate reduction due to ethanol oxidation is:



where the subscript (S) indicates SRB. The net rate of growth of SRB is related to the rate of sulfate consumption by:

$$\begin{aligned} \frac{dX_S}{dt} = & Y_{SO_4} \frac{q_{\max,SO_4} c_{EtOH}}{K_{EtOH,S} + c_{EtOH}} \frac{c_{SO_4}}{K_{SO_4} + c_{SO_4}} \frac{K_{NO_3}}{K_{NO_3} + c_{NO_3}} X_S - b_N X_S \frac{c_{NO_3}}{K_{NO_3} + c_{NO_3}} \\ & - b_S X_S \frac{c_{SO_4}}{K_{SO_4} + c_{SO_4}} \frac{K_{NO_3}}{K_{NO_3} + c_{NO_3}} - b_U X_S \frac{c_{U(VI)}^*}{K_{U(VI)} + c_{U(VI)}^*} \frac{K_{NO_3}}{K_{NO_3} + c_{NO_3}} \end{aligned} \quad (10)$$

where Y_{SO_4} is the yield coefficient for sulfate-reducing bacteria [$M_x M_s^{-1}$] and q_{\max,SO_4} is the maximum specific rate of substrate utilization for sulfate [$M_s M_x^{-1} T^{-1}$]. Like in biomass decay, the term $K_{NO_3}/(K_{NO_3} + c_{NO_3})$ expresses the inhibition of sulfate reduction in the presence of nitrate. Sulfate is also consumed in the decay of both denitrifiers and SRB in the absence of nitrate. The reaction of biomass decay with sulfate as an electron acceptor is:



The rate of sulfate reduction thus is:

$$\begin{aligned} \frac{dc_{SO_4}}{dt} = & -q_{\max,SO_4} F_{SO_4,EtOH} X_S \frac{c_{EtOH}}{K_{EtOH,NO_3} + c_{EtOH}} \frac{c_{SO_4}}{K_{SO_4} + c_{SO_4}} \frac{K_{NO_3}}{K_{NO_3} + c_{NO_3}} \\ & - d_{SO_4} f_d (b_S X_N + b_S X_S) \frac{c_{SO_4}}{K_{SO_4} + c_{SO_4}} \frac{K_{NO_3}}{K_{NO_3} + c_{NO_3}} \end{aligned} \quad (11)$$

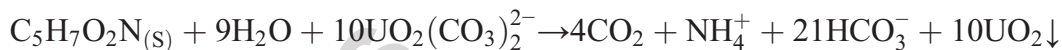
where d_{SO_4} is the sulfate demand for cell decay [MM_x^{-1}], and $F_{SO_4,EtOH}$ is the stoichiometric ratio of sulfate to ethanol utilization for biomass synthesis [MM_s^{-1}].

3.5. Uranium reduction

Uranyl–carbonate complexes are the primary bioavailable compounds in aqueous solution. The U(VI) reduction due to ethanol consumption can be written as (Abdelouas et al., 2000):



Based on experiments with source-zone sediment and artificial groundwater, sulfate-reducing bacteria are likely to be responsible for microbial U(VI) reduction at the site (Nyman et al., 2005). The equation for biomass decay with uranium-carbonate complexes as an electron acceptor is:



As U(VI) is assumed to be respired concurrently by SRB, U(VI) reduction kinetics is expected to follow saturation kinetics with respect to the biomass concentration of SRB:

$$\begin{aligned} \frac{dc_{U(VI)}^*}{dt} = & -q_{\max,U(VI)} X_S \frac{c_{U(VI)}^*}{K_{U(VI)} + c_{U(VI)}^*} \frac{c_{EtOH}}{K_{EtOH,U(VI)} + c_{EtOH}} \frac{K_{NO_3}}{K_{NO_3} + c_{NO_3}} \\ & - d_{U(VI)} f_d (b_U X_N + b_U X_S) \frac{c_{U(VI)}^*}{K_{U(VI)} + c_{U(VI)}^*} \frac{K_{NO_3}}{K_{NO_3} + c_{NO_3}} \end{aligned} \quad (12)$$

where $q_{\max,U(VI)}$ is the maximum effective rate for uranium reduction [$MM_x^{-1} T^{-1}$], $d_{U(VI)}$ is the uranium demand for the cell decay [MM_x^{-1}]. Eq. (12) assumes the bioavailable U(VI) can be reduced by biomass decay of both denitrifiers and sulfate-reducing bacteria (Wu et al., 2005).

3.6. Ethanol consumption

Ethanol serves as the electron donor for denitrification, sulfate reduction, and U(VI) reduction. In this model, ethanol is assumed to be completely degraded and the production and consumption

of intermediates such as acetate are not considered in the model. Then, the reactive source/sink term for ethanol is given by:

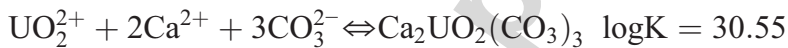
$$\begin{aligned} \frac{dc_{\text{EtOH}}}{dt} = & -q_{\text{max,NO}_3} X_N \frac{c_{\text{EtOH}}}{K_{\text{EtOH,NO}_3} + c_{\text{EtOH}}} \frac{c_{\text{NO}_3}}{K_{\text{NO}_3} + c_{\text{NO}_3}} \\ & - q_{\text{max,SO}_4} X_S \frac{c_{\text{EtOH}}}{K_{\text{EtOH,SO}_4} + c_{\text{EtOH}}} \frac{c_{\text{SO}_4}}{K_{\text{SO}_4} + c_{\text{SO}_4}} \frac{K_{\text{NO}_3}}{K_{\text{NO}_3} + c_{\text{NO}_3}} \\ & - q_{\text{max,U(VI)}} X_S \frac{c_{\text{EtOH}}}{K_{\text{EtOH,U(V)}} + c_{\text{EtOH}}} \frac{c_{\text{U(VI)}}^*}{K_{\text{U(VI)}} + c_{\text{U(VI)}}^*} \frac{K_{\text{NO}_3}}{K_{\text{NO}_3} + c_{\text{NO}_3}} \end{aligned} \quad (13)$$

3.7. Parameters

Table 1 summarizes the parameters used in the bioreactive models. Most of them are taken from the literature, or are a result of the stoichiometry of the reactions, where mass balance has been obeyed for all elements. The kinetic parameters for sulfate reduction are determined by laboratory experiments. The effective value of $q_{\text{max,U(VI)}}$ is uncertain and is estimated by fitting the in-situ experiment. b_U is assumed to be equivalent to b_N and b_S .

3.8. Uranium(VI) aqueous and surface chemistry

Our database for aqueous U(VI) speciation includes the compilation of Grenthe et al. (1992), amended by the calcium–uranyl–carbonate complexes (Bernhard et al., 1996; Kalmykov and Choppin, 2000; Bernhard et al., 2001), in which U(VI) is considered less bioavailable (Brooks et al., 2003):



Aqueous speciation of all elements other than U is based on the Wateq4f database (Ball and Nordstrom, 1991).

We have implemented a principal-component surface complexation model to describe U(VI) interaction with the saprolite matrix over a range of pH and concentrations of competing ions. Studying sorption of U(VI) onto uncontaminated saprolite at the site, Barnett et al. (2002) demonstrated that U(VI) uptake is dominated by sorption to Fe(III) oxyhydroxide phases in this matrix and that its extent can be described in first approximation by applying a surface complexation model developed independently by Waite et al. (1994) for U(VI) adsorption onto ferrihydrite. Following their approach, we assume all dithionite–citrate–bicarbonate extractable Fe (23.1 g/kg saprolite) to be present as active sorbent phases resembling ferrihydrite-like surface properties. To describe competitive ion sorption, we implemented the diffuse double layer surface complexation model using the database compiled by Dzombak and Morel (1990), who adopted 0.2 mol weak and 0.005 mol strong sorption sites per mol Fe, $\text{p}K_{\text{a1}}=7.29$, $\text{p}K_{\text{a2}}=-8.93$, and a surface area of 600 m²/g of ferrihydrite. The major surface reactions and input parameters included in our model are summarized in Table 2, which are those deemed most important. Formation constants of surface carbonate complexes are from Appelo et al. (2002). For U(VI) sorption we implemented the bidentate uranyl and ternary uranyl–carbonate surface complexes proposed by Waite et al. (1994) based on EXAFS spectroscopy, but refitted their formation

Table 2

Surface reactions and log equilibrium constants for surface complexation of uranium onto ferric iron (hydr)oxide

Surface reactions	Log K	References
<i>Uranyl and uranyl–carbonate surface complexes</i>		
$2\equiv\text{Fe}_w\text{OH}+\text{UO}_2^{2+}\leftrightarrow(\equiv\text{Fe}_w\text{O})_2\text{UO}_2+2\text{H}^+$	-4.80	Fitted
$2\equiv\text{Fe}_s\text{OH}+\text{UO}_2^{2+}\leftrightarrow(\equiv\text{Fe}_s\text{O})_2\text{UO}_2+2\text{H}^+$	-2.58	Fitted
$2\equiv\text{Fe}_w\text{OH}+\text{UO}_2^{2+}+\text{CO}_3^{2-}\leftrightarrow(\equiv\text{Fe}_w\text{O})_2\text{UO}_2\text{CO}_3^{2-}+2\text{H}^+$	-3.49	Fitted
$2\equiv\text{Fe}_s\text{OH}+\text{UO}_2^{2+}+\text{CO}_3^{2-}\leftrightarrow(\equiv\text{Fe}_s\text{O})_2\text{UO}_2\text{CO}_3^{2-}+2\text{H}^+$	3.94	Fitted
<i>Other surface complexation reactions</i>		
$\equiv\text{Fe}_{s,w}\text{OH}+\text{H}^+\leftrightarrow\equiv\text{Fe}_{s,w}\text{OH}_2^+$	7.29	Dzombak and Morel (1990)
$\equiv\text{Fe}_{s,w}\text{OH}\leftrightarrow\equiv\text{Fe}_{s,w}\text{O}^-+\text{H}^+$	-8.93	Dzombak and Morel (1990)
$\equiv\text{Fe}_w\text{OH}+\text{CO}_3^{2-}+\text{H}^+\leftrightarrow\equiv\text{Fe}_w\text{OCO}_2^-+\text{H}_2\text{O}$	12.78	Appelo et al. (2002)
$\equiv\text{Fe}_w\text{OH}+\text{CO}_3^{2-}+2\text{H}^+\leftrightarrow\equiv\text{Fe}_w\text{OCO}_2\text{H}+\text{H}_2\text{O}$	20.37	Appelo et al. (2002)

constants to be consistent with the ferrihydrite parameters of Dzombak and Morel (1990) and our thermodynamic database. We fitted all $n_f=4$ U(VI) surface complexes simultaneously to the $n_d=128$ recorded data points of Waite et al. (1994) for uranyl sorption at various pH, U(VI)/ferrihydrite ratios, partial CO_2 pressure, and ionic strength. n_f is the number of fitted parameters and n_d the number of measured data points. Fitting was conducted using PHREEQC (Parkhurst and Appelo, 1995) nested into an iterative MATLAB routine minimizing the root mean square error (RMSE) according to:

$$\text{RMSE} = \left[\frac{1}{n_d - n_f} \sum_{i=1}^{n_d} \left(\frac{c_m(\text{pH}_i) - c_{\text{calc}}(\text{pH}_i)}{c_{\text{tot}}} \right)^2 \right]^{0.5} \quad (14)$$

where c_m and c_{calc} are the measured and calculated aqueous U(VI) concentrations, respectively, at the i -th measured pH value under system equilibrium, and c_{tot} is the total U(VI) concentration in the experiment. The obtained formation constants given in Table 2 resulted in a good fit (RMSE=8.6%), but for the highest U(VI) to Fe molar ratio of 0.1. At such high U(VI) loading possibly surface precipitation occurs in addition to surface complexation. During the biostimulation experiment such ratios are not expected. Payne et al. (1996) and Cheng et al. (2004) presented evidence for the formation of ternary uranyl-phosphate surface complexes. As they seem to form mainly under acidic conditions, shifting the lower sorption edge to lower pH, we have not yet included them in our model.

The fractions of sorption sites in the mobile and immobile domains, f_m and f_{im} , are fitting parameters to the specific field site conditions. Kinetic sorption/desorption is controlled by mass transfer between the mobile and immobile domains. This approach is similar to the strategy used by Roden and Scheibe (2005).

4. Results and discussion

4.1. Overall performance

Fig. 3 shows measured concentrations at the injection well FW104 and at the observation point FW101–2, as well as simulated concentrations at FW101–2. The measurements at the injection well FW104 are considered as input functions. Initial concentrations are assumed uniformly distributed over the domain with values of the initial measurements at FW101–2. We simulate three phases of

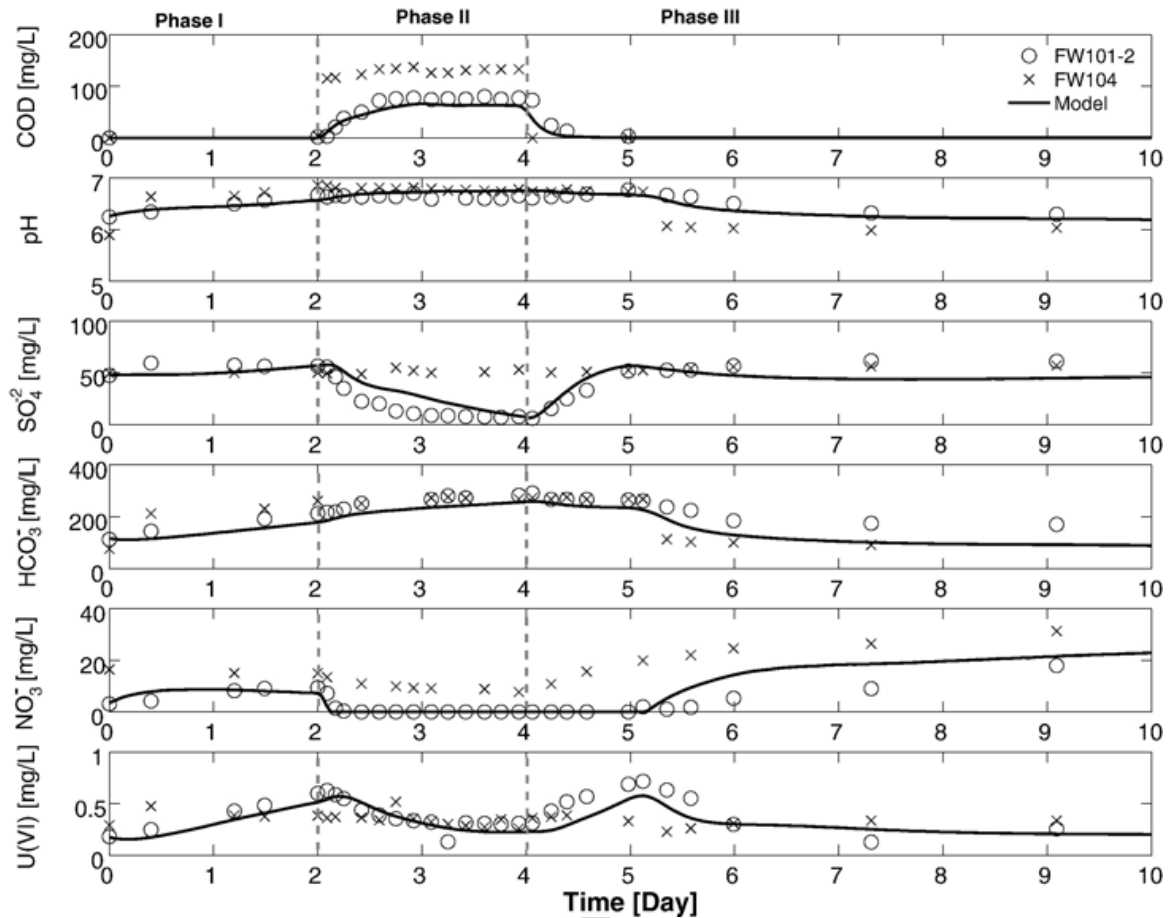


Fig. 3. Model simulation and measurements at FW101–2. Concentrations measured at FW104 are input functions, and those at FW101–2 are response functions. The grey dashed lines delineate the phase II of ethanol injection.

the experiment: in phase 1, K_2CO_3 was injected to increase pH; in phase 2, ethanol was injected to stimulate biomass growth; and phase 3 was after termination of ethanol injection. During the experiment, all water extracted from the extraction well FW026 was reinjected in FW104. The measurements from injection well FW104 were taken in the well, thus dilution within the well need not to be considered in the model. Parameters estimated by fitting the model include: the effective value of maximum specific rate of U(VI) reduction, $q_{\max,U(VI)} = 1 \text{ mM}_{U(VI)}/\text{mg}_{SRB}\text{-day}$, and the fractions of sorption sites in the mobile and immobile domains, $f_m = 0.013$ and $f_{im} = 0.987$. The physical interpretation of these parameters will be discussed in the following sections. Fig. 3 shows that the proposed model performs satisfactory in reproducing the trends of the major components in this reactive system although significant simplifications for the hydrogeochemical conditions have been assumed. The overall RMSE evaluated by Eq. (14) is 4.1%.

4.2. Inhibition by nitrate

The concentration profiles of nitrate, sulfate and U(VI) in Fig. 3 indicate the succession of terminal electron-accepting processes during the experiment. Although most nitrate was removed by preconditioning the aquifer and biological denitrification for more than 200 days (Wu et al., 2006a), nitrate concentrations, at the start of this biostimulation experiment, were still at levels that could negatively impact the reduction of sulfate and U(VI) due to release of trapped nitrate from the soil matrix and infiltration of nitrate from outside the inner recirculation loop. For the fast

flow zone, we assume that the time needed to remove all nitrate could be over 1 year without in-situ denitrification (Luo et al., 2005). Operational results indicated that nitrate remains at significant concentrations (2–10 mM) in the slow-flow area and may re-enter the treatment zone by recirculation. Due to ethanol amendment in phase II, nitrate was consumed quickly by denitrification in the mobile domain. Ethanol therefore first stimulated the growth of denitrifying biomass. The growth of SRB was stimulated after the completion of denitrification, as evidenced by a decrease in sulfate concentration. Together with sulfate, U(VI) was reduced. Phase III further demonstrated the succession of terminal electron-accepting processes. After terminating the ethanol injection, sulfate and U(VI) concentrations increased immediately due to injection of recirculated groundwater, desorption and mass transfer from stagnant pores. Contrarily, nitrate concentration had a time lag for rebounding because biomass decay of denitrifiers and SRB utilized nitrate as electron acceptor. During this time lag, pH and bicarbonate concentration were almost constant. We conclude that experimental design must consider the consumption of electron donors by denitrification in the experimental design.

In the proposed reactive transport model, we account for the inhibition of sulfate and U(VI) reduction by nitrate with the inhibition term $K_{\text{NO}_3}/(K_{\text{NO}_3} + c_{\text{NO}_3})$. This approach approximates the general competitive inhibition model (Rittmann and McCarty, 2001)

$$\frac{c_{\text{EtOH}}}{K_{\text{EtOH,NO}_3} \left(1 + \frac{c_{\text{NO}_3}}{K_{i,\text{NO}_3}}\right) + c_{\text{EtOH}}} \quad (15)$$

using

$$\frac{c_{\text{EtOH}}}{K_{\text{EtOH,SO}_4} + c_{\text{EtOH}}} \frac{K_{\text{NO}_3}}{K_{\text{NO}_3} + c_{\text{NO}_3}} \quad (16)$$

Eq. (15) needs one more unknown parameter, K_{i,NO_3} , than Eq. (16). However, the exact value of K_{i,NO_3} is not significant in our simulation because the concentration profiles show that sulfate and U(VI) reduction requires almost complete removal of nitrate, indicating a small value of K_{i,NO_3} . Thus, the proposed model, Eq. (16), can characterize the inhibition effects over a large range of nitrate concentrations. When nitrate concentration drops to low levels, the two models may differ. However, the influences are not significant for this field-scale simulation, especially as our case is not electron-donor limiting during the biostimulation.

4.3. U(VI) sorption/desorption

As a result of aquifer conditioning, the aqueous U(VI) concentrations decreased from about 50 mg/l to 0.5 mg/l. Most of U(VI) sorbed onto the aquifer solids or resided in the immobile domains, which cannot be reached easily by acidic flushing. Thus, during the experiment, sorption/desorption mechanisms determine the bioavailability of U(VI). The fitted sorption site fractions, $f_m=0.013$ and $f_{im}=0.987$, indicate that almost all sorption sites are associated with the immobile domain. This result may be in part an artifact caused by the model's description of transport and sorption kinetics. The surface complexation model implemented in PHREEQC assumes local sorption equilibrium in both the mobile and immobile domains, while the exchange of U(VI) between the immobile and mobile domains is controlled by kinetic mass transfer. Thus, the fitted fraction values may partly represent sorption site distribution and partly account for the effects of kinetic sorption/desorption of U(VI). In this simulation, the mass transfer coefficients,

λ_m and λ_{im} , are assumed to be $5 \times 10^{-5}/s$, a mean value determined by column and field tracer studies (Luo et al., 2005). Therefore, the half-life of the time scale for kinetic sorption/desorption assumed in this model is about 4 h.

The model simulation confirms that it may not be valid to use a simple empirical isotherm, such as a linear partitioning coefficient, for the description of U(VI) sorption/desorption during U(VI) bioreduction. pH and bicarbonate concentration, known as two major factors controlling U(VI) sorption/desorption mechanisms (Waite et al., 1994; Wazne et al., 2003), vary over the course of the experiment. In phase I, with the increase of bicarbonate concentration, U(VI) desorbed from the solid phase, resulting in the increase of aqueous U(VI) concentrations in the mobile domain. In phase II, denitrification and sulfate reduction produced additional bicarbonate, which may have caused continuing desorption of U(VI). However, in this phase, the rate of bioreduction was presumably larger than that of desorption, so that concentrations of U(VI) decreased. In the initial time of phase III (day 4–day 5), when pH and bicarbonate concentration were almost constant, U(VI) concentrations increased because of kinetic desorption and inhibited reduction. Later in phase III, when pH and bicarbonate concentration decreased, U(VI) concentrations decreased because of less desorption from the solids. Over time in this biostimulation experiment, U(VI) sorption/desorption changed with pH and bicarbonate concentrations. Thus, a constant isotherm cannot adequately characterize this mechanism.

4.4. U(VI) reduction

U(VI) reduction accompanied sulfate reduction via mainly enzymatic reduction. The fitted effective reduction rate is $q_{\max, U(VI)} = 1 \text{ mM}_{U(VI)}/\text{mg}_{\text{SRB}}\text{-day}$, which is much smaller than reported for laboratory experiments. Spear et al. (1999) determined the U(VI) reduction rates

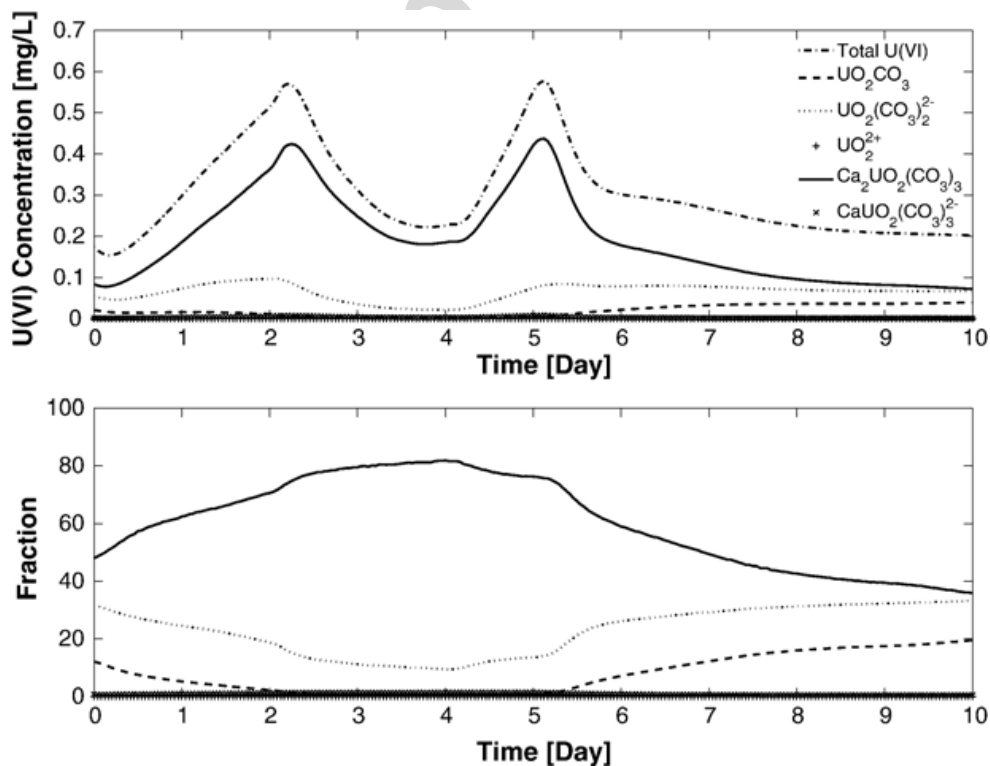


Fig. 4. Concentrations and fractions of aqueous U(VI) species with the consideration of calcium–uranyl–carbonate complexes.

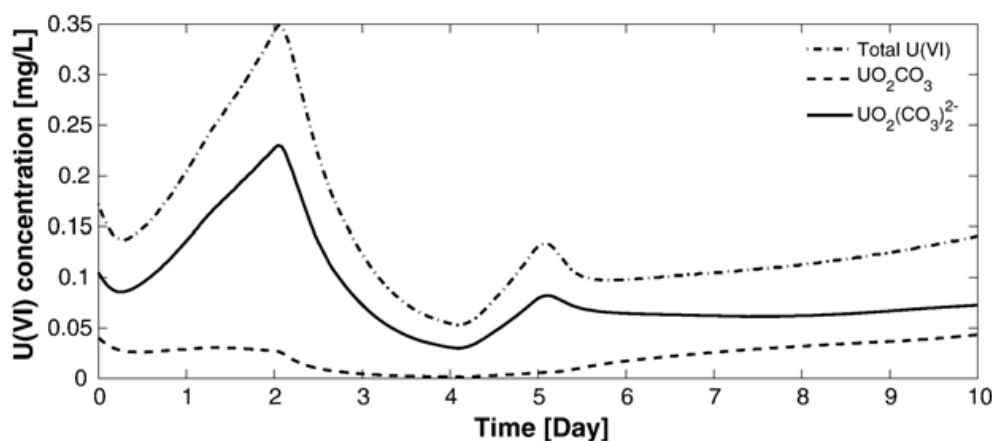


Fig. 5. Species concentrations for the simulation without calcium–uranyl–carbonate complexes.

43.2 $\text{mM}_{\text{U(VI)}}/\text{mg}_{\text{SRB-day}}$ for *Desulfovibrio desulfuricans* and 31.7 $\text{mM}_{\text{U(VI)}}/\text{mg}_{\text{SRB-day}}$ for mixed culture of SRB under non-growth conditions. Our results indicate dramatic differences between field-scale experiments and well-controlled laboratory experiments, reflecting the effects of complicated field conditions. Because oxidation of reduced uranium is not considered in the reaction kinetics, the effective value represents the net rate of U(VI) reduction. U(VI) reduction is not only controlled by electron donor and sulfate concentrations and bioreduction rate, but also by the bioavailability of U(VI), that is, by the kinetics of mass transfer of U(VI) between the mobile and immobile domains.

Fig. 4 shows the simulated concentration and fraction profiles of aqueous U(VI) species. In phase I, all U(VI) species concentrations increased due to U(VI) desorption. The dominant aqueous species is the calcium–uranyl–carbonate complex, $\text{Ca}_2\text{UO}_2(\text{CO}_3)_3$. With U(VI) desorption, its fraction kept increasing because of its high stability. As already mentioned, calcium–uranyl–carbonate complexes are practically unavailable for bioreduction thermodynamically (Brooks et al., 2003). Although its concentration decreased in phase II, its fraction slowly increased due to chemical equilibrium. According to our simulations, the major bioavailable species is $\text{UO}_2(\text{CO}_3)_2^{2-}$. In phase III, all species fractions recovered with decreases of pH and bicarbonate concentrations. Fig. 5 shows the species concentrations for a simulation neglecting the calcium–uranium–carbonate complexes using otherwise identical parameters. The model predicts that soluble U(VI) would have decreased to much lower levels as a result of biostimulation. This comparison indicates that the high stability of calcium–

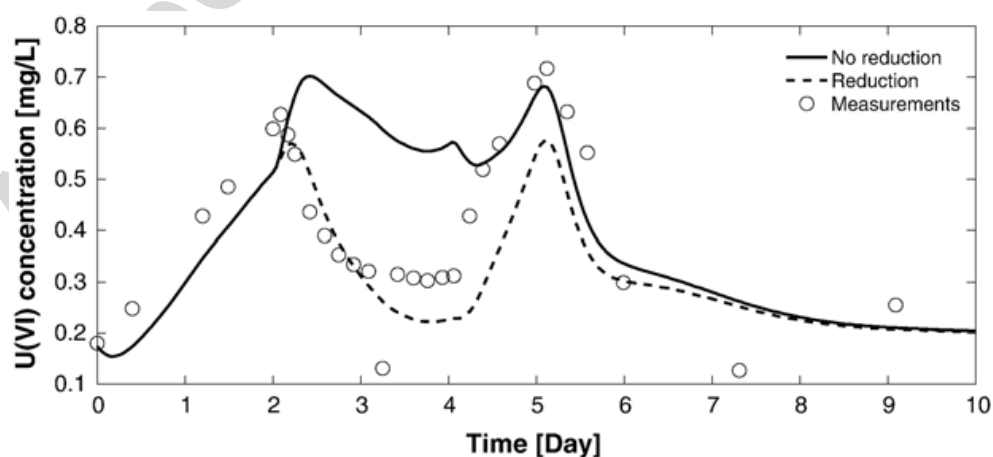


Fig. 6. Comparison of total U(VI) concentrations at FW101–2 for the U(VI) reduction case and no-reduction case.

uranyl–carbonate complexes significantly influences the effective bioreduction of U(VI). We conclude that strategies are needed to decrease calcium concentrations in the design of uranium bioremediation.

Fig. 6 compares the simulation with and without U(VI) reduction, i.e., $q_{\max, \text{U(VI)}}=0$. Significant reduction can be observed during the ethanol injection phase II. In phase I, U(VI) concentrations of both cases are larger than the input U(VI) at the injection well FW104, indicating that the produced bicarbonate concentrations mobilized the sorbed U(VI). Thus, pH, bicarbonate, and calcium concentrations are the important factors controlling the bioavailability of U(VI).

5. Conclusions

Modeling in-situ U(VI) bioreduction requires the consideration of uranium aqueous chemistry, uranium sorption/desorption, and bioreactive kinetics. In the presence of nitrate, the succession of terminal electron-accepting processes needs to be accounted for. We present a model including an inhibition term $K_{\text{NO}_3}/(K_{\text{NO}_3} + c_{\text{NO}_3})$ to quantify the inhibitory effects of nitrate on sulfate and U(VI) reduction. This approach avoids the determination of the unknown inhibition parameter and characterizes the field data well. However, for small-scale problems, more accurate models may be needed, especially for characterizing at which values the electron-accepting processes switch from one to the other. The reduction rate of U(VI) is not only controlled by the injection of electron donor, but also significantly influenced by the sorption/desorption rates, which are mainly controlled by the levels of pH and bicarbonate concentration. Since pH and bicarbonate concentrations vary over the course of the experiment, models assuming simple sorption/desorption isotherms may not adequately characterize these mechanisms. Surface complexation models are more effective to describe the U(VI) sorption/desorption by including the calculations of aqueous speciation and surface complexes. In PHREEQC, surface complexation is implemented as equilibrium process, thus lacking sorption kinetics. We have circumvented this shortcoming by using a mobile–immobile transport model, fitting the sorption site distributions to represent the kinetic processes. The model results indicate significant kinetic effects of U(VI) sorption/desorption. Calcium–uranyl–carbonate complexes are very important for modeling the aqueous equilibrium state and determining the bioavailable U(VI) concentrations. Although the role of FeRB in U(VI) cannot be ruled out, we do not include it in our current model because of its relatively low population observed in MLS well FW101–2. Extending our model to multiple types of biomass would be straightforward.

Models for in-situ U(VI) bioreduction involve many uncertain parameters, including those of aqueous U(VI) speciation, surface complexation and bioreaction kinetics. Thus, for efficient applications, sensitivity analysis is needed to simplify the models, such as presented by Wang et al. (2003). Thorough characterization of the hydrological and geochemical conditions will also help improve the model performance. For this site, we had a long period of preconditioning operations (Wu et al., 2006a), and within the bioremediation experiment, uncontrolled and unexpected factors disturbed the long-term experiment. Thus, it is difficult to use a detailed and all-encompassing model to simulate the whole period of experiments. As shown by Wu et al. (2006b), the behavior of measured breakthrough curves shows periodic characteristics with the overall U(VI) exhibiting a decreasing trend. Thus, we select one period with good measurements to test the model. Although significant assumptions are made, the model characterized the measured data well. Furthermore, re-oxidation of immobilized uranium needs to be included in future models to evaluate the long-term success of bioreduction techniques (Abdelouas et al., 1999; Finneran et al., 2002).

Acknowledgement

This work was partially funded by the Environmental Remediation Sciences Program (ERSP) of the USA Department of Energy (DOE) grant number (#DE-F603-00ER63046). The authors thank H. Yan, K. Lowe and Dr. B. Gu for analytical support, T. Mehlhorn for field work, M. Fienen and M. Gentile for valuable suggestions and comments on modeling, and T.E. Payne for providing us with the uranyl adsorption data of Waite et al. (1994) in an electronic format. The authors appreciate the assistance of Paul Bayer, the ERSP program manager, and David Watson, FRC site manager. We thank two anonymous reviewers for their constructive comments to this manuscript.

References

- Abdelouas, A., Lu, Y., Lutze, W., Nuttall, H.E., 1998. Reduction of U(VI) to U(IV) by indigenous bacteria in contaminated ground water. *J. Contam. Hydrol.* 35 (1–3), 217–233.
- Abdelouas, A., Lutze, W., Nuttall, E.H., 1999. Oxidative dissolution of uraninite precipitated on Navajo sandstone. *J. Contam. Hydrol.* 36, 353–375.
- Abdelouas, A., Lutze, W., Gong, W., Nuttall, E.H., Strietelmeier, B.A., Travis, B.J., 2000. Biological reduction of uranium in groundwater and subsurface soil. *Sci. Total Environ.* 250, 21–35.
- Almeida, J.S., Reis, M.A.M., Carronda, M.J.T., 1997. A unifying kinetic model of denitrification. *J. Theor. Biol.* 186 (2), 241–249.
- Anderson, R.T., Lovley, D.R., 2002. Microbial redox interactions with uranium: an environmental perspective. *Interactions of Micro-Organisms with Radionuclides*. Elsevier Science Ltd.
- Appelo, C.A.J., van der Weiden, M.J.J., Tournassat, C., Charlet, L., 2002. Surface complexation of ferrous iron and carbonate on ferrihydrite and the mobilization of arsenic. *Environ. Sci. Technol.* 36, 3096–3103.
- Bain, J.G., Mayer, K.U., Blowes, D.W., Frind, E.O., Molson, J.W.H., Kahnt, R., Jenk, U., 2001. Modelling the closure-related geochemical evolution of groundwater at a former uranium mine. *J. Contam. Hydrol.* 52, 109–135.
- Ball, J.W., Nordstrom, D.K., 1991. WATEQ4F—user’s manual with revised thermodynamic data base and test cases for calculating speciation of major, trace and redox elements in natural waters. U.S. Geological Survey Open-File, pp. 90–129.
- Barnett, M.O., Jardine, P.M., Brooks, S.C., 2002. Uranium(VI) adsorption to heterogeneous subsurface media: application of a surface complexation model. *Environ. Sci. Technol.* 36, 937–942.
- Bernhard, G., Geipel, G., Brendler, V., Nitsche, H., 1996. Speciation of uranium in seepage waters of a mine tailing pile studied by time-resolved laser-induced fluorescence spectroscopy (TRLFS). *Radiochim. Acta* 74, 87–91.
- Bernhard, G., Geipel, G., Reich, T., Brendler, V., Amayri, S., Nitsche, H., 2001. Uranyl(VI) carbonate complex formation: validation of the $\text{Ca}_2\text{UO}_2(\text{CO}_3)_3$ species. *Radiochim. Acta* 89 (8), 511–518.
- Betlach, M.R., Tiedje, J.M., 1981. Kinetic explanation for accumulation of nitrite, nitric-oxide, and nitrous-oxide during bacterial denitrification. *Appl. Environ. Microbiol.* 42 (6), 1074–1084.
- Brooks, S.C., Fredrickson, J.K., Carroll, S.L., Kennedy, D.W., Zachara, J.M., Plymale, A.E., Kelly, S.D., Kemner, K.M., Fendorf, S., 2003. Inhibition of bacterial U(VI) reduction by calcium. *Environ. Sci. Technol.* 37, 1850–1858.
- Cheng, T., Barnett, M.O., Roden, E.E., Zhuang, J., 2004. Effects of phosphate on uranium(VI) adsorption to goethite-coated sand. *Environ. Sci. Technol.* 38 (22), 6059–6065.
- Cirpka, O.A., Kitanidis, P.K., 2000. Travel-time based model of bioremediation using circulation wells. *Ground Water* 39, 422–432.
- Crane, M.J., Blunt, M.J., 1999. Streamline-based simulation of solute transport. *Water Resour. Res.* 35 (10), 3061–3078.
- Davis, J.A., Coston, J.A., Kent, D.B., Fuller, C.C., 1998. Application of the surface complexation concept to complex mineral assemblages. *Environ. Sci. Technol.* 32 (19), 2820–2828.
- Davis, J.A., Meece, D.E., Kohler, M., Curtis, G.P., 2004. Approaches to surface complexation modeling of uranium(VI) adsorption on aquifer sediments. *Geochim. Cosmochim. Acta* 68 (18), 3621–3641.
- Dzombak, D.A., Morel, F.M.M., 1990. *Surface Complexation Modeling: Hydrous Ferric Oxide*. John Wiley and Sons, New York.
- Fienen, M.N., Kitanidis, P.K., Watson, D., Philip, P.M., 2004. An application of bayesian inverse methods to vertical deconvolution of hydraulic conductivity in a heterogeneous aquifer at Oak Ridge National Laboratory. *Math. Geol.* 36 (1), 101–126.

- Finneran, K.T., Housewright, M.E., Lovley, D.R., 2002. Multiple influences of nitrate on uranium solubility during bioremediation of uranium-contaminated subsurface sediments. *Environ. Microbiol.* 4 (9), 510–516.
- Fredrickson, J.K., Zachara, J.M., Kennedy, D.W., Duff, M.C., Gorby, Y.A., Li, S.W., Krupka, K.M., 2000. Reduction of U(VI) in goethite (FeOOH) suspensions by a dissimilatory metal-reducing bacterium. *Geochim. Cosmochim. Acta* 64 (18), 3085–3098.
- Fredrickson, J.K., Zachara, J.M., Kennedy, D.W., Liu, C., Duff, M.C., Hunter, D.B., Dohnalkova, A., 2002. Influence of Mn oxides on the reduction of uranium(VI) by the metal-reducing bacterium *Shewanella putrefaciens*. *Geochim. Cosmochim. Acta* 66 (18), 3247–3262.
- Froelich, P.N., Klinkhammer, G.P., Bender, M.L., Luedtke, N.A., Heath, G.R., Cullen, D., Dauphin, P., Hammond, D., Hartman, B., Maynard, V., 1979. Early oxidation of organic matter in pelagic sediments of the eastern equatorial Atlantic: suboxic diagenesis. *Geochim. Cosmochim. Acta* 43, 1075–1090.
- Ganesh, R., Robinson, K.G., Reed, G.D., Sayler, G.S., 1997. Reduction of hexavalent uranium from organic complexes by sulfate- and iron-reducing bacteria. *Appl. Environ. Microbiol.* 63 (11), 4385–4391.
- Giammar, D.E., Hering, J.G., 2001. Time scales for sorption: desorption and surface precipitation of uranyl on goethite. *Environ. Sci. Technol.* 35 (16), 3332–3337.
- Gorby, Y.A., Lovley, D.R., 1992. Enzymatic uranium precipitation. *Environ. Sci. Technol.* 26 (1), 205–207.
- Grenthe, I., Fuger, J., Konings, R.J.M., Lemire, R.J., Muller, A.B., Nguyen-Trung, C., Wanner, H. (Eds.), 1992. *Chemical Thermodynamics of Uranium*. Nuclear Energy Agency OECD. Elsevier Science Publishers.
- Holmes, D.E., Finneran, K.T., O'Neil, R.A., Lovley, D.R., 2002. Enrichment of members of the family Geobacteraceae associated with stimulation of dissimilatory metal reduction in uranium-contaminated aquifer sediments. *Appl. Environ. Microbiol.* 68 (5), 2300–2306.
- Hsi, C.D., Langmuir, D., 1985. Adsorption of uranyl onto ferric oxyhydroxide: application of the surface complexation site-binding model. *Geochim. Cosmochim. Acta* 49, 1931–1941.
- Kalmykov, S.N., Choppin, G.R., 2000. Mixed $\text{Ca}^2/\text{UO}_2/\text{CO}_2$ complex formation at different ionic strengths. *Radiochim. Acta* 88 (9–11), 603–606.
- Kohler, M., Curtis, G.P., Kent, D.B., Davis, J.A., 1996. Experimental investigation and modeling of uranium(VI) transport under variable chemical conditions. *Water Resour. Res.* 32, 3539–3551.
- Liger, E., Charlet, L., Van Cappelin, P., 1999. Surface catalysis of uranium(VI) reduction by iron(II). *Geochim. Cosmochim. Acta* 63, 2939–2955.
- Liu, C., Kota, S., Zachara, J.M., Fredrickson, J.K., Brinkman, C.K., 2001. Kinetic analysis of the bacterial reduction of goethite. *Environ. Sci. Technol.* 35, 2482–2490.
- Lovley, D.R., Phillips, E.J.P., 1992a. Reduction of uranium by *Desulfovibrio desulfuricans*. *Appl. Environ. Microbiol.* 58 (3), 850–856.
- Lovley, D.R., Phillips, E.J.P., 1992b. Bioremediation of uranium contamination with enzymatic uranium reduction. *Environ. Sci. Technol.* 26 (11), 2228–2234.
- Lovley, D.R., Phillips, E.J.P., Gorby, Y.A., Landa, E.R., 1991. Microbial reduction of uranium. *Nature* 350, 413–415.
- Luo, J., Cirpka, O.A., Wu, W., Fienen, M.N., Jardine, P.M., Mehlhorn, T.L., Watson, D.B., Criddle, C.S., Kitanidis, P.K., 2005. Mass-transfer limitation for nitrate removal in a uranium-contaminated aquifer. *Environ. Sci. Technol.* 39 (21), 8453–8459.
- Luo, J., Cirpka, O.A., Fienen, M.N., Wu, W.-M., Mehlhorn, T.L., Carley, J., Jardine, P.M., Criddle, C.S., Kitanidis, P.K., 2006a. A parametric transfer function methodology for analyzing reactive transport in nonuniform flow. *J. Contam. Hydrol.* 83 (1–2), 27–41.
- Luo, J., Wu, W., Fienen, M.N., Jardine, P.M., Mehlhorn, T.L., Watson, D.B., Cirpka, O.A., Criddle, C.S., Kitanidis, P.K., 2006b. A nested-cell approach for in situ remediation. *Ground Water* 44 (2), 266–274.
- McCarty, P.L., 1975. Stoichiometry of biological reactions. *Prog. Water Technol.* 7 (1), 157–172.
- McKinley, J.P., Zachara, J.M., Smith, S.C., Turner, G.D., 1995. The influence of uranyl hydrolysis and multiple site-binding reactions on adsorption of U(VI) to montmorillonite. *Clays Clay Miner.* 43, 586–598.
- Morrison, S.J., Spangler, R.R., Tripathi, V.S., 1995. Adsorption of uranium(VI) on amorphous ferric oxyhydroxide at high concentrations of dissolved carbon(IV) and sulfur(VI). *J. Contam. Hydrol.* 17, 333–346.
- Nagpal, S., Chuichulcherm, S., Livingston, A., Peeva, L., 2000. Ethanol utilization by sulfate-reducing bacteria: an experimental and modeling study. *Biotechnol. Bioeng.* 70 (5), 533–543.
- North, N.N., Dollhopf, S.L., Petrie, L., Istok, J.D., Balkwill, D.L., Kostka, J.E., 2004. Change in bacterial community structure during in situ biostimulation of subsurface sediment cocontaminated with uranium and nitrate. *Appl. Environ. Microbiol.* 70 (8), 4911–4920.
- Nyman, J.L. 2006. Community structure and kinetics of microbial uranium reduction for field-scale bioremediation. Ph.D. Dissertation. Stanford University.

- Nyman, J.L., Williams, S.M., Criddle, C.S., 2005. Bioengineering for the in situ remediation of metals. Environmental Catalysis. CRC Press.
- Nyman, J.L., Marsh, T.L., Ginder-Vogel, M.A., Gentile, M., Fendorf, S., Criddle, C.S., 2006. Heterogeneous response to biostimulation for U(VI) reduction in replicated sediment microcosms. *Biodegradation* 17 (4), 303–316.
- Parkhurst, D.L., Appelo, C.A.J., 1995. User's guide to PHREEQC-A computer program for speciation, reaction-path, advective-transport, and inverse geochemical calculations. U.S. Geological Survey Water-Resources Investigations, pp. 95–4227.
- Parks, G.A., Pohl, D.C., 1988. Hydrothermal solubility of uraninite. *Geochim. Cosmochim. Acta* 52, 863–875.
- Payne, T.E., Davis, J.A., Waite, T.D., 1996. Uranium adsorption on ferrihydrite—effects of phosphate and humic acid. *Radiochim. Acta* 74, 239–243.
- Phillips, D.H., Watson, D.B., Roh, Y., Mehlhorn, T.L., Moon, J.-W., Jardine, P.M., 2006. Distribution of uranium contamination in weathered fractured saprolite/shale and groundwater. *J. Environ. Qual.* 35, 1715–1730.
- Prikryl, J.D., Pabalan, R.T., Turner, D.R., Leslie, B.W., 1994. Uranium sorption on-alumina: effects of pH and surface area/solution–volume ratio. *Radiochim. Acta* 66/67, 291–296.
- Prikryl, J.D., Jain, A., Truner, D.R., Pabalan, R.T., 2001. Uranium(VI) sorption behavior on silicate mineral mixtures. *J. Contam. Hydrol.* 47, 241–253.
- Qafoku, N.P., Zachara, J.M., Liu, C., Gassman, P.L., Qafoku, O.S., Smith, S.C., 2005. Kinetic desorption and sorption of U(VI) during reactive transport in a contaminated Hanford sediment. *Environ. Sci. Technol.* 39 (9), 3157–3165.
- Reeburgh, W.S., 1983. Rates of biogeochemical processes in anoxic sediments. *Annu. Rev. Earth Planet. Sci.* 31, 28–36.
- Roden, E.E., Scheibe, T.D., 2005. Conceptual and numerical model of uranium(VI) reductive immobilization in fractured subsurface sediments. *Chemosphere* 59 (5), 617–628.
- Rittmann, B.E., McCarty, P.L., 2001. *Environmental Biotechnology: Principles and Applications*. McGraw-Hill, New York.
- Senko, J.M., Istok, J.D., Sufliata, J.M., Krumholz, L.R., 2002. In-situ evidence for uranium immobilization and remobilization. *Environ. Sci. Technol.* 36 (7), 1491–1496.
- Simmons, C.S., Ginn, T., Wood, B., 1995. Stochastic-convective transport with nonlinear reaction: mathematical framework. *Water Resour. Res.* 31 (11), 2675–2688.
- Spear, J.R., Figueroa, L.A., Honeyman, B.D., 1999. Modeling the removal of uranium U(VI) from aqueous solutions in the presence of sulfate reducing bacteria. *Environ. Sci. Technol.* 33 (15), 2667–2675.
- Spear, J.R., Figueroa, L.A., Honeyman, B.D., 2000. Modeling reduction of uranium U(VI) under variable sulfate concentrations by sulfate-reducing bacteria. *Appl. Environ. Microbiol.* 66 (9), 3711–3721.
- Tripathi, V.S. 1984. Uranium(VI) transport modeling: geochemical data and submodels. Ph.D. Dissertation. Stanford Univ., CA.
- Truex, M.J., Peyton, B.M., Valentine, N.B., Gorby, Y.A., 1997. Kinetics of U(VI) reduction by a dissimilatory Fe(III)-reducing bacterium under non-growth conditions. *Biotechnol. Bioeng.* 55 (3), 490–496.
- Turner, G.D., Zachara, J.M., McKinley, J.P., Smith, S.C., 1996. Surface-charge properties and UO₂²⁺ adsorption of a subsurface smectite. *Geochim. Cosmochim. Acta* 60, 3399–3414.
- Waite, T.D., Davis, J.A., Payne, T.E., Waychunas, G.A., Xu, N., 1994. Uranium(VI) adsorption to ferrihydrite: application of a surface complexation model. *Geochim. Cosmochim. Acta* 58, 5465–5478.
- Wang, Y., Papenguth, H.W., 2001. Kinetic modeling of microbially-driven redox chemistry of radionuclides in subsurface environments: coupling transport, microbial metabolism and geochemistry. *J. Contam. Hydrol.* 47 (2–4), 297–309.
- Wang, S., Jaffe, P.R., Li, G., Wang, S.W., Rabitz, H.A., 2003. Simulating bioremediation of uranium-contaminated aquifers; uncertainty assessment of model parameters. *J. Contam. Hydrol.* 64, 283–307.
- Wazne, M., Korfiatis, G.P., Meng, X.G., 2003. Carbonate effects on hexavalent uranium adsorption by iron oxyhydroxide. *Environ. Sci. Technol.* 37 (16), 3619–3624.
- Weber, F.-A., 2002. Reactive transport modeling: stimulation of microbial uranium(VI) reduction for remediation of a contaminated aquifer. Thesis, University of Stuttgart, Germany.
- Wersin, P., Hochella Jr., M.F., Persson, P., Redden, G., Leckie, J.O., Harris, D.W., 1994. Interaction between aqueous uranium(VI) and sulfide minerals: spectroscopic evidence for sorption and reduction. *Geochim. Cosmochim. Acta* 58, 2829–2843.
- Wielinga, B., Bostick, B., Hansel, C.M., Rosenzweig, R.F., Fendorf, S., 2000. Inhibition of bacterially promoted uranium reduction: Ferric (hydr)oxides as competitive electron acceptors. *Environ. Sci. Technol.* 34 (11), 2190–2195.
- Wu, W.-M., Gu, B., Fields, M.W., Gentile, M., Ku, Y.-K., Yan, H., Tiquias, S., Yan, T., Nyman, J., Zhou, J., Jardine, P.M., Criddle, C.S., 2005. Uranium (VI) reduction by denitrifying biomass. *Bioremediat. J.* 9 (1), 1–13.
- Wu, W.-M., Carley, J., Fienen, M., Mehlhorn, T., Lowe, K., Nyman, J., Luo, J., Gentile, M.E., Rajan, R., Wagner, D., Hickey, R.F., Gu, B., Watson, D., Cirpka, O., Kitanidis, P., Jardine, J., Criddle, C.S., 2006a. Pilot-scale in situ

bioremediation of uranium in a highly contaminated aquifer. 1. Conditioning of a treatment zone. *Environ. Sci. Technol.* 40 (12), 3978–3985.

Wu, W.-M., Carley, J., Gentry, T., Ginder-Vogel, M.A., Fienen, M., Mehlhorn, T., Yan, H., Carroll, S., Nyman, J., Luo, J., Gentile, M.E., Fields, M.W., Hickey, R.F., Gu, B., Watson, D., Fendorf, S., Zhou, J., Kitanidis, P., Jardine, P.M., Criddle, C.S., 2006b. Pilot-scale in situ bioremediation of uranium in a highly contaminated aquifer. 2. Reduction of U(VI) and geochemical control of U(VI) bioavailability. *Environ. Sci. Technol.* 40 (12), 3986–3995.

Author's personal copy